nature biomedical engineering

ARTICLES

https://doi.org/10.1038/s41551-018-0252-8

Nanoparticle delivery of CRISPR into the brain rescues a mouse model of fragile X syndrome from exaggerated repetitive behaviours

Bumwhee Lee[1,4], Kunwoo Lee[2,4], Shree Panda[1], Rodrigo Gonzales-Rojas[1], Anthony Chong[2], Vladislav Bugay[1], Hyo Min Park[2], Robert Brenner[1], Niren Murthy[3]* and Hye Young Lee[1]*

Technologies that can safely edit genes in the brains of adult animals may revolutionize the treatment of neurological diseases and the understanding of brain function. Here, we demonstrate that intracranial injection of CRISPR–Gold, a nonviral delivery vehicle for the CRISPR–Cas9 ribonucleoprotein, can edit genes in the brains of adult mice in multiple mouse models. CRISPR–Gold can deliver both Cas9 and Cpf1 ribonucleoproteins, and can edit all of the major cell types in the brain, including neurons, astrocytes and microglia, with undetectable levels of toxicity at the doses used. We also show that CRISPR–Gold designed to target the metabotropic glutamate receptor 5 (mGluR5) gene can efficiently reduce local mGluR5 levels in the striatum after an intracranial injection. The effect can also rescue mice from the exaggerated repetitive behaviours caused by fragile X syndrome, a common single-gene form of autism spectrum disorders. CRISPR–Gold may significantly accelerate the development of brain-targeted therapeutics and enable the rapid development of focal brain-knockout animal models.

Programmable RNA-guided endonucleases have the potential to revolutionize the treatment of neurological diseases because of their ability to cut genes with sequence specificity[1–5]. Despite their potential, the translational impact of RNA-guided endonucleases on the central nervous system has been limited due to challenges in performing efficient gene editing in adult brains with minimal toxicity. Currently, gene editing in the adult brain is mainly accomplished through the viral delivery of clustered regularly interspaced short palindromic repeats (CRISPR)–CRISPR-associated protein 9 (Cas9)[6]. However, the translation of viral delivery methods for CRISPR–Cas9 and single guide RNA (sgRNA) in the brain can be challenging because of the immunogenicity of viruses[7] and the genomic damage caused from the prolonged expression of CRISPR–Cas9 and sgRNA[8]. Moreover, the toxicity caused from the continuous expression of foreign proteins in neurons, which frequently causes changes in neuronal phenotypes[9], is a challenge. Therefore, there is great interest in developing nonviral methods for delivering RNA-guided endonucleases into the brains of adult mice. However, very little is known about the ability of RNA-guided endonucleases to transfect the brains of adult animals via nonviral methods. Currently, there is only one report of nonviral gene editing in the adult brain, which used an intracranial injection of Cas9 ribonucleoproteins (RNPs) engineered with multiple nuclear localization sequence (NLS) signals[10]. In addition, there are no reports of nonviral gene editing in the brain with RNA-guided endonucleases beyond Cas9, making it unclear whether other RNA-guided endonucleases, such as CRISPR from *Prevotella* and *Francisella* 1 (Cpf1), can perform gene editing in the adult brain via nonviral delivery methods.

A wide number of neurological diseases could potentially be treated with gene editing-based therapeutics. Of these, fragile X syndrome (FXS) is a particularly attractive target for gene editing-based therapeutics because of the current lack of therapeutic options and the high morbidity that this disease causes. FXS is an autism-associated single-gene mutation-based disorder, which is driven by a repeat expansion mutation in the fragile X mental retardation 1 (*FMR1*) gene, which encodes the fragile X mental retardation protein (FMRP), an mRNA-binding protein[11]. FXS is the most common inherited form of intellectual disability and a common single-gene form of autism spectrum disorders (ASDs), accounting for ~2.1% of patients[12]. Current drug treatments, such as psychostimulants, antidepressants and antipsychotics, are ineffective because they do not address the underlying aetiology of FXS; they only target individual symptoms[13,14]. In addition, current FXS pharmacotherapies cause severe side effects such as weight gain and sedation[14]. New treatments for FXS are urgently needed; however, developing FXS treatments based on traditional small molecules has been challenging because of the limited number of validated FXS therapeutic targets and the difficulties associated with developing therapeutics that can provide long-term effectiveness without causing cytotoxicity to brain cells.

CRISPR-based editing of the brain, generated by a local intracranial injection, has great potential for treating FXS because it will lead to localized gene editing in the brain. Consequently, the patient is spared the the toxic effects of globally inhibiting neuronal signalling pathways. In addition, CRISPR gene editing is permanent and would make repeated injections unnecessary, making it feasible in a variety of clinical scenarios. There are several genes that are potential targets for a CRISPR-based FXS therapy; of these, mGluR5 is particularly attractive because its exaggerated signalling has been demonstrated to be associated not only with FXS but also with other ASDs[15–20]. The importance of modulating mGluR5 in ASDs triggered several pharmaceutical companies to develop small molecule-based therapies that target mGluR5; however, these small molecules

[1]The Department of Cellular and Integrative Physiology, University of Texas Health Science Center at San Antonio, San Antonio, TX, USA. [2]GenEdit Inc., Berkeley, CA, USA. [3]Department of Bioengineering, University of California, Berkeley, Berkeley, CA, USA. [4]These authors contributed equally: Bumwhee Lee, Kunwoo Lee. *e-mail: nmurthy@berkeley.edu; leeh6@uthscsa.edu

failed in clinical trials[21,22]. Therefore, knocking out the mGluR5 gene (*Grm5*) locally in brain regions that are hypothesized to cause the behavioural phenotypes in patients with FXS has great potential for treating FXS and autism-related disorders. However, several questions need to be answered before gene editing can become a therapeutic treatment for FXS. First, the delivery challenges associated with gene editing in the brain with Cas9 RNPs, as described above, need to be solved. Second, it is unclear whether mGluR5-mediated behavioural phenotypes are caused by focal overactivation of mGluR5 signalling and, if so, which parts of the brain need to have the exaggerated mGluR5 signalling reduced to ameliorate a specific behavioural phenotype.

Here, we investigated whether a recently developed nonviral Cas9 delivery vehicle, termed CRISPR–Gold[23], could deliver the RNA-guided endonucleases Cas9 and Cpf1 into the brains of adult mice and we performed gene editing in Thy1-YFP and Ai9 mice. We then targeted the mGluR5 gene to reduce the exaggerated mGluR5 signalling in the striatum of a mouse model of FXS. We show that the CRISPR–Gold-mediated mGluR5 reduction rescued striatum-dependent exaggerated repetitive behaviours, as measured by the marble-burying assay and jumping behaviour of the mice. Our results demonstrate that CRISPR–Gold has the potential to significantly accelerate the development of new brain-targeted therapeutics. Moreover, this platform can enable the rapid development of focal brain-knockout models for mechanistic, brain region or preclinical studies given its ability to edit genes in adult brains via the nonviral delivery of Cas9 RNPs.

Results

Biocompatibility test of CRISPR–Gold in neurons. Nonviral delivery vehicles that can edit genes in the brain have great potential for treating neurological disorders. However, very little is known about nonviral gene editing in the brain. We identified CRISPR–Gold (Fig. 1a) as a potential delivery vector for gene editing in the brain because it was able to efficiently deliver Cas9 RNPs into a variety of cell types in vitro and into mouse muscles[23]. To investigate the biocompatibility of CRISPR–Gold in neuronal cells, we measured the cytotoxicity and physiological effects of primary cultured hippocampal neurons treated with CRISPR–Gold loaded with Cas9 RNPs (the formation of the CRISPR–Gold complex was verified, as shown in Supplementary Fig. 1). The concentration of CRISPR–Gold applied to the neuronal cells was 25 pmole per 0.5 ml for both Cas9 and sgRNAs, 17 ng per 0.5 ml of gold, and 2.5 μg per 0.5 ml of PAsp(DET). Two hours after treatment, the residual CRISPR–Gold was removed and replaced with fresh growth medium plus conditioned medium (50:50). After 10–14 days of CRISPR–Gold treatment, neurons were patch-clamped or stained with SYTOX Red to count dead cells. We first checked the electrophysiological properties (whole-cell current clamp recording) of pyramidal neurons after treatment with CRISPR–Gold. The results showed that there was no difference in the membrane potentials between control and treated neurons (Fig. 1b). Input resistance, which in part indicates the leakiness of the plasma membrane, in the treated neurons was not significantly different from the untreated neurons (Fig. 1c). Consistent with the input resistance result, the number of spikes generated by a 200 pA current injection did not significantly change in CRISPR–Gold-treated neurons (summarized in Fig. 1d, representative traces in Fig. 1e). Therefore, we conclude that CRISPR–Gold treatment does not have adverse effects on neuronal membrane health or specifically affect neuronal excitability. We then stained dead cells with SYTOX and visualized cell morphology by co-staining actin with a phalloidin stain to check the cytotoxicity of CRISPR–Gold treatment. No significant differences in the number of dead cells and neuronal morphology were found in CRISPR–Gold-treated cells compared with untreated neurons (Fig. 1f). Taken together, our results show that treatment with CRISPR–Gold is neither cytotoxic nor does it affect the physiological function of neurons under the conditions tested here. However, we do not know the elimination kinetics of the gold nanoparticle (GNP) core of CRISPR–Gold from neurons or whether extended retention of the gold core in neurons leads to toxicity.

CRISPR–Gold-mediated gene editing in the brains of Thy1-YFP mice. To test our idea of whether CRISPR–Gold could deliver Cas9 RNPs in an adult mouse brain, we stereotaxically injected CRISPR–Gold into the brains of adult mice (Fig. 2a). We selected neurons as the initial target for gene editing investigations because of their essential function in brain activities and their strong correlation with a wide variety of neurological diseases. The Thy1-YFP mouse model, a transgenic mouse line that expresses YFP only in neurons and not in other types of brain cells[24], was used to monitor gene editing in neurons (Fig. 2a). The sgRNAs for Cas9 and CRISPR RNAs (crRNAs) for Cpf1 were designed to target the 5′ region of the YFP gene to induce insertion/deletion (indel) mutations (Supplementary Fig. 2a). These guide RNAs were verified by checking the YFP gene knockout capability in YFP-expressing HEK cells (Supplementary Fig. 2b–d). CRISPR–Gold loaded with Cas9 or Cpf1 RNPs targeting the 5′ region of the YFP gene was then injected into the dentate gyrus in the hippocampus of 1–2-month-old adult mice (Fig. 2b). Figure 2c,d and Supplementary Fig. 3 show that CRISPR–Gold can deliver Cas9 and Cpf1 RNPs and efficiently edit the YFP gene in neurons that are projecting to the molecular layer of the dentate gyrus after the stereotaxic injection of CRISPR–Gold with Cas9 or Cpf1 RNPs. As a result, there was an ~17% and ~28% decrease in YFP^+ cells in the granular layer of the dentate gyrus by Cas9 and Cpf1, respectively (Fig. 2c,d). Moreover, there was a 34% and 25% decrease in YFP expression levels (Supplementary Fig. 3a,b) in the molecular layer of the dentate gyrus after the delivery of Cas9 and Cpf1, respectively. These results demonstrate that Cas9 and Cpf1, delivered by CRISPR–Gold, are efficient methods for local in vivo editing in the brain. Interestingly, modulating small subpopulations of neurons (200–300 neurons) in focal brain regions has been shown to change behavioural outputs[25,26]. CRISPR–Gold may therefore be able to treat neurological disorders and elucidate the function of genes in brain circuits, despite only editing a small fraction of the total number of brain cells after an intracranial injection.

CRISPR–Gold-mediated gene editing in the brains of Ai9 mice. Gene editing via deletion of repeated genetic sequences in a human brain can be a potential cure for disorders such as Huntington disease and FXS, which have repeated sequences that result in brain dysfunctions[27–29]. Therefore, we performed experiments in Ai9 mice to determine whether Cas9 and Cpf1 RNPs could induce genome editing by deleting a target gene in an adult mouse brain (Figs. 3a,b and 4a). The Ai9 mouse is a genetically engineered mouse model that has a fluorescent tdTomato gene with a stop sequence upstream of it[30]. In this mouse model, tdTomato is silent because of the stop signal, but the deletion of the stop sequences allows transcription of the tdTomato gene, resulting in fluorescence expression (Fig. 3a). sgRNAs for Cas9 and crRNAs for Cpf1 were designed to target both ends of the stop sequences to remove them, leading to the expression of tdTomato (Supplementary Fig. 4a). These guide RNAs were verified in primary fibroblasts cultured from Ai9 mice, and were able to induce the expression of tdTomato (Supplementary Fig. 4b). Cas9- or Cpf1-loaded CRISPR–Gold was stereotaxically injected into two brain regions (the hippocampus and the striatum of 1–2-month-old adult Ai9 mice as shown in Figs. 3b and 4a), and the expression of tdTomato was measured via fluorescence histology.

Figure 3c,d demonstrates that both Cas9 and Cpf1 CRISPR–Gold complexes can induce deletion of their target sequences and can induce the expression of tdTomato in the CA1 region of the hippocampus of Ai9 mice. For example, fluorescence histology images

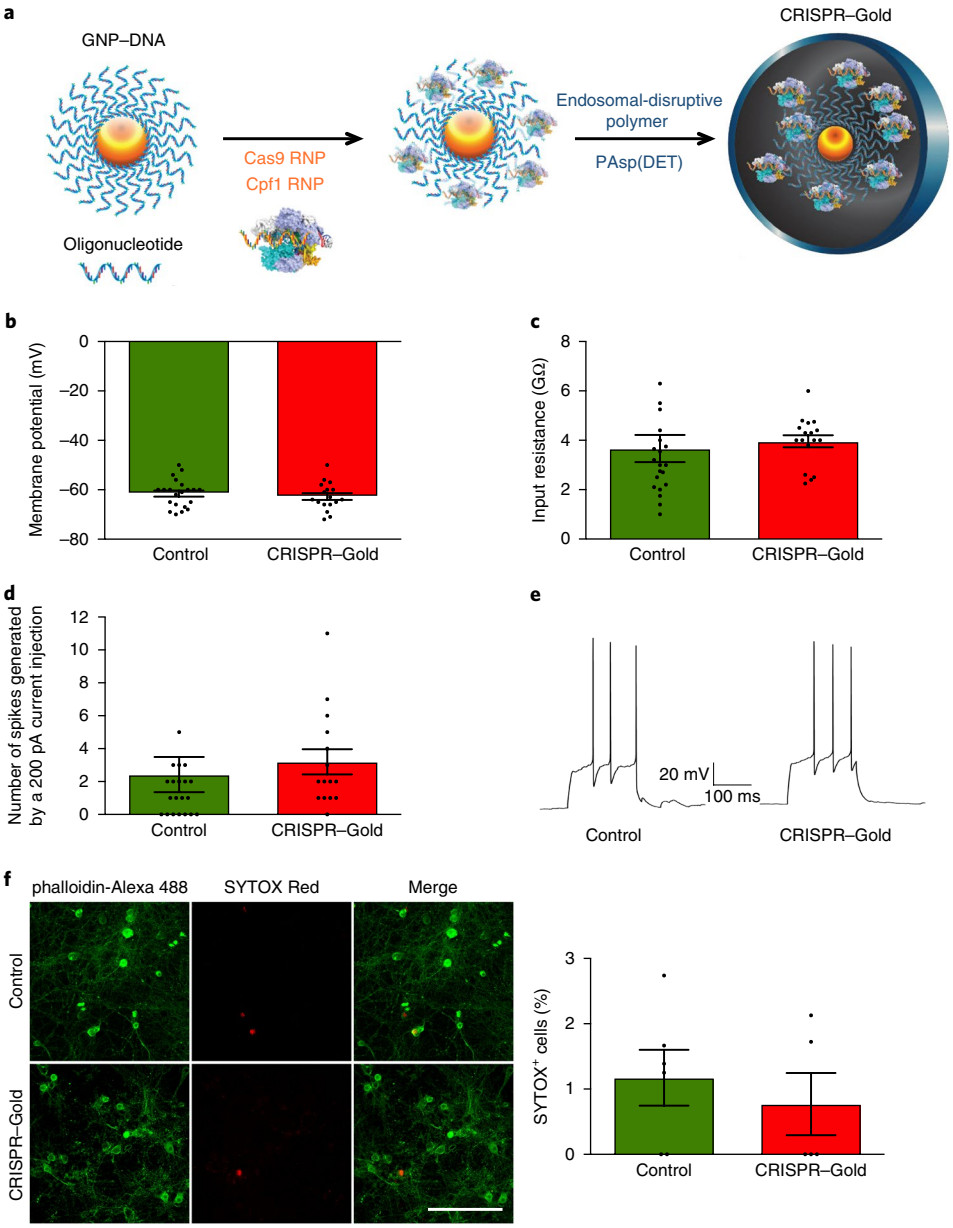

Fig. 1 | No significant physiological deficit or cytotoxicity is found in primary cultured neurons after CRISPR–Gold treatment. a, Schematic of CRISPR–Gold synthesis. DNA oligonucleotide-conjugated GNPs bind to Cas9 or Cpf1 RNPs, and subsequent PAsp(DET) polymer encapsulation generates CRISPR–Gold. **b**-**d**, Primary cultured neurons (days in vitro 7 (DIV7)) were treated with CRISPR–Gold Cas9 RNPs (CRISPR–Gold) and were compared with untreated neurons (control) for electrophysiological properties by whole-cell current clamp recording. Neurons were measured for membrane potential (**b**), input resistance (**c**) and the number of spikes generated by a 200 pA current injection (**d**). $n = 20$–21 for control, $n = 15$–17 for CRISPR–Gold, mean ± s.e.m. No significant differences in the membrane potentials, input resistance or the number of spikes were found between the groups. **e**, Representative traces for control and CRISPR–Gold. **f**, Left: DIV7 primary cultured neurons were treated with CRISPR–Gold Cas9 RNPs (CRISPR–Gold) and were compared with untreated neurons (control). Neurons were fixed 14 days after CRISPR–Gold treatment and stained with SYTOX Red to identify dead cells (red) and with phalloidin-Alexa 488 for visualizing neuronal morphology (green). Scale bar, 100 μm. Right: quantification of SYTOX$^+$ cells (%) among DAPI$^+$ cells in the control and CRISPR–Gold groups. $n = 6$ for control, $n = 5$ for CRISPR–Gold, mean ± s.e.m. No significant difference in the percentage of SYTOX$^+$ cells was found between groups. This experiment was replicated twice.

of the hippocampus area treated with Cas9 or Cpf1 CRISPR–Gold complexes showed clear expression of tdTomato compared with the contralateral control side (Fig. 3c,d). Approximately 10–15% of the cells in the injected area of the hippocampus were tdTomato$^+$ in both Cas9 and Cpf1 RNP-injected brains; these cells were quantified by analysing the percentage of cells stained positive for both tdTomato and 4,6-diamidino-2-phenylindole (DAPI) (Fig. 3c,d). Similar results were found in the striatum (Fig. 4b,c). For example, tdTomato is clearly expressed in the striatum after an injection of Cas9 or Cpf1 CRISPR–Gold complexes compared with the contralateral control side (Fig. 4b,c). Approximately 10% of the cells in the injected area of the striatum were tdTomato$^+$ in both Cas9 and Cpf1 RNP-injected brains (Fig. 4b,c). These results suggest that Cas9 and Cpf1 RNPs can efficiently delete targeted DNA sequences using the CRISPR–Gold delivery vehicle. The gene-edited area was 1–2 mm × 1–2 mm for the hippocampus and striatum from the injection sites, and within these regions, there was no observable change in cell density by counting DAPI$^+$ cells (Fig. 4d,e), indicating

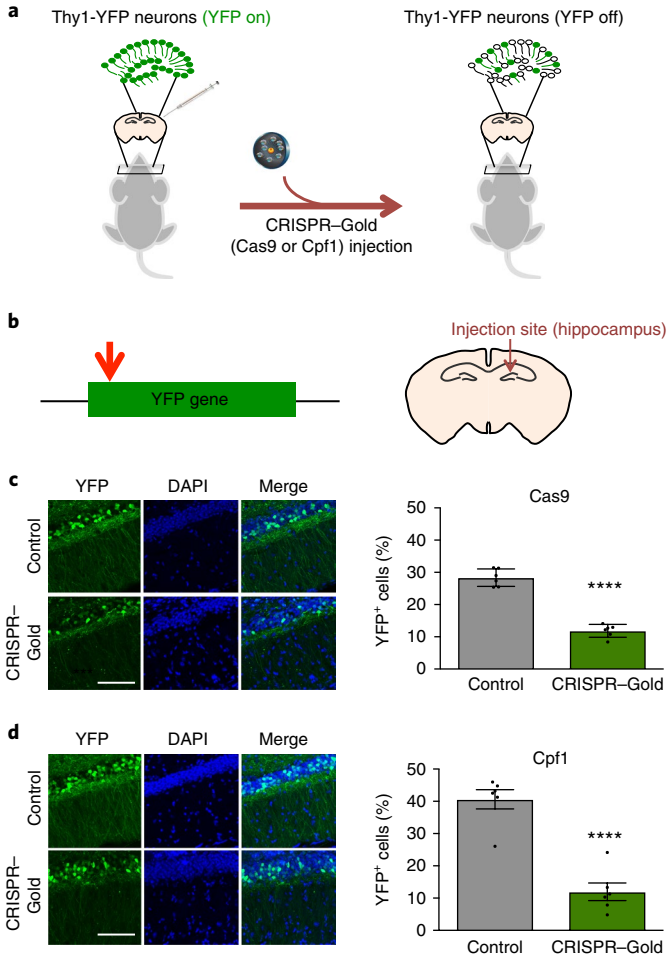

Fig. 2 | YFP expression is efficiently reduced in the neurons of the mouse brain using CRISPR–Gold delivery of Cas9 or Cpf1 RNPs in Thy1-YFP mice. a, Schematic of CRISPR–Gold delivery of Cas9 or Cpf1 RNPs into the brains of Thy1-YFP mice. **b**, Left: schematic of Cas9 or Cpf1 RNP-mediated indel mutation. Red arrow indicates the target region for gene-editing. Right: schematic of stereotaxic injection into the hippocampus (Bregma: −2.18 mm) of Thy1-YFP mice using the CRISPR–Gold system. **c**,**d**, Left: immunostaining of YFP-labelled neurons (green) with nuclei staining with DAPI (blue) 2 weeks after stereotaxic injection of Cas9 (**c**) or Cpf1 (**d**) RNPs using the CRISPR–Gold system into the dentate gyrus of the hippocampus of Thy1-YFP mice. Scale bars, 100 μm. Right: quantification of the YFP$^+$ cells normalized to DAPI$^+$ cell numbers in the granule cell layer of the dentate gyrus in the injected side (CRISPR–Gold) compared with the contralateral control side (control). $n = 6$ for each group, mean ± s.e.m., $^{****}P < 0.0001$ compared with the control side, Student's unpaired t-test. This experiment was replicated four times.

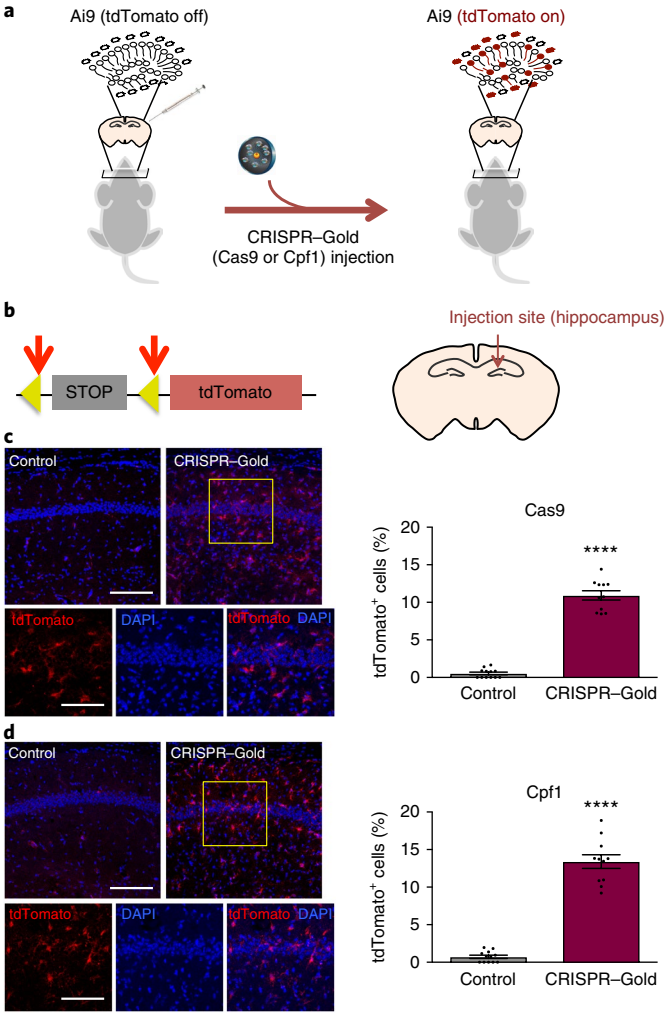

Fig. 3 | Deletion of stop sequences and expression of tdTomato in the brain of Ai9 mice by CRISPR–Gold delivery of Cas9 or Cpf1 RNPs into the hippocampus. a, Schematic of CRISPR–Gold delivery of Cas9 or Cpf1 RNPs into the brains of Ai9 mice. **b**, Left: schematic of Cas9 or Cpf1 RNP-mediated deletion. Yellow arrowheads represent the 5′ and 3′ ends of the stop sequence. Red arrows indicate target regions for gene editing. Right: schematic of stereotaxic injection into the hippocampus (Bregma: −2.18 mm) of Ai9 mice using the CRISPR–Gold system. **c**,**d**, Left: immunostaining of tdTomato (red) and nuclei staining with DAPI (blue) 2 weeks after stereotaxic injection of Cas9 (**c**) or Cpf1 (**d**) RNPs using the CRISPR–Gold system into the hippocampus of Ai9 mice. The uninjected side (control) and the injected side (CRISPR–Gold) are shown in the upper panels. Scale bars, 200 μm. Higher-magnification images of the injected side (yellow box) are shown in the lower panels. Scale bars, 100 μm. Right: quantification of the percentage of tdTomato$^+$ cells among DAPI$^+$ cells in the Cas9 RNP-injected area (**c**) and the Cpf1 RNP-injected area (**d**). $n = 11$–12 for each group, mean ± s.e.m., $^{****}P < 0.0001$ compared with the control side, Student's unpaired t-test. This experiment was replicated twice.

that cell viability is not significantly adversely affected. A potential limitation of CRISPR–Gold is its GNP core, which can potentially accumulate in the brain and cause toxicity. However, the gold core constitutes a minor fraction of the total weight of CRISPR–Gold, and the dose of gold used in the mouse experiments was ~2.84 μg kg^{-1}, which is orders of magnitude lower than the toxicity threshold for GNPs in the brain[31,32].

CRISPR–Gold-mediated gene editing in multiple cell types. Neurons are the basic working units of the brain, whereas non-neuronal cells play a central role in maintaining, supporting and regulating neuronal functions. Glial cell dysfunction causes multiple brain disorders[33], and there is great interest in editing the genes of glial cells. Therefore, we used Ai9 mice to further identify the brain cell types edited by Cas9 or Cpf1 RNPs delivered by CRISPR–Gold and to determine whether glial cells were edited. CRISPR–Gold-injected Ai9 brain sections were stained with the following cell markers: glial fibrillary acidic protein (GFAP), ionized calcium-binding adapter molecule 1 (IBA1) and neuronal nuclear protein (NeuN). GFAP, IBA1 and NeuN identify the astrocyte, microglia and neuronal populations, respectively, in histology sections.

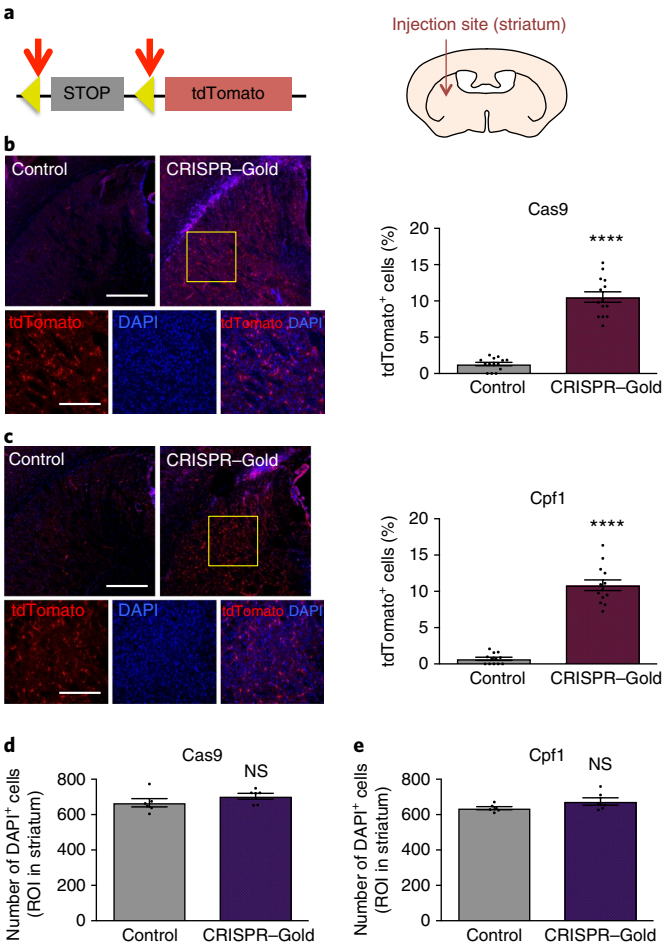

Fig. 4 | Deletion of stop sequences and expression of tdTomato in the brain of Ai9 mice by CRISPR–Gold delivery of Cas9 or Cpf1 RNPs into the striatum. a, Left: schematic of Cas9 or Cpf1 RNP-mediated deletion. Yellow arrowheads represent the 5′ and 3′ ends of the stop sequence. Red arrows indicate target regions for gene editing. Right: schematic of stereotaxic injection into the striatum (Bregma: 0.26 mm) of Ai9 mice using the CRISPR–Gold system. **b**,**c**, Left: immunostaining of tdTomato (red) and nuclei staining with DAPI (blue) 2 weeks after stereotaxic injection of Cas9 (**b**) or Cpf1 (**c**) RNPs using the CRISPR–Gold system into the striatum of Ai9 mice. The uninjected side (control) and the injected side (CRISPR–Gold) are shown in the upper panels. Scale bars, 400 μm. Higher-magnification images of the injected side (yellow box) are shown in the lower panels. Scale bars, 200 μm. Right: quantification of the percentage of tdTomato$^+$ cells among DAPI$^+$ cells in the Cas9 RNP-injected area (**b**; $n = 14$ for each group, mean ± s.e.m.) and Cpf1 RNP-injected area (**c**; $n = 12$–13 for each group, mean ± s.e.m.). ****$P < 0.0001$ compared with the control side, Student's unpaired t-test. This experiment was replicated twice. **d**,**e**, Quantification of the number of DAPI$^+$ cells in the Cas9 (**d**) or Cpf1 RNP-injected area (striatum) (**e**). Two weeks after stereotaxic injection of Cas9 or Cpf1 RNPs using the CRISPR–Gold system into the striatum of Ai9 mice, the brains were sliced and immunostained with tdTomato antibodies and stained with DAPI. The number of DAPI$^+$ cells of equal size in the injected ROI of the striatum in both the control group and the CRISPR–Gold group were compared and analysed. $n = 6$ for each group, mean ± s.e.m., NS, not significant, Student's unpaired t-test. This experiment was replicated twice.

Supplementary Figures 5 and 6 demonstrate that gene-edited tdTomato-expressing cells were composed of all three of these cell types (astrocytes, microglia and neurons). In the hippocampus, more than half of the tdTomato$^+$ cells had the astrocyte marker GFAP in Cas9 or Cpf1 RNP-injected brains, and IBA1- and NeuN-stained cells accounted for approximately 40% and 10% of the tdTomato$^+$ cells, respectively (Supplementary Fig. 5b,d, left panels). This result suggests that astrocytes, microglia and neurons are edited by CRISPR–Gold Cas9 and Cpf1 in the hippocampus. Similar results were found in the striatum. In the striatum of brains injected with Cas9 or Cpf1, more than half of the tdTomato$^+$ cells had the astrocyte marker GFAP. In addition, cells stained with IBA1 and NeuN accounted for 10–30% of tdTomato$^+$ cells in brains injected with Cas9 or Cpf1 (Supplementary Fig. 6b,d, left panels). In the hippocampus of brains injected with Cas9, 33% of GFAP$^+$, 19% of IBA1$^+$ and 3% of NeuN$^+$ cells were edited among astrocytes, microglia and neurons (Supplementary Fig. 5b, right panels). For Cpf1, 65% of GFAP$^+$, 21% of IBA1$^+$ and 5% of NeuN$^+$ cells were edited among astrocytes, microglia and neurons (Supplementary Fig. 5d, right panels). Similar results were found in the striatum, with 50% (Cas9) and 46% (Cpf1) of GFAP$^+$, 18% (Cas9) and 14% (Cpf1) of IBA1$^+$, and 3% (Cas9) and 7% (Cpf1) of NeuN$^+$ cells edited among astrocytes, microglia and neurons (Supplementary Fig. 6b,d, right panels). Taken together, these results demonstrate that CRISPR–Gold-delivered Cas9 and Cpf1 RNPs can induce deletion of target genes in the major cell types of the brain, including astrocytes, microglia and neurons.

Gene editing in *Fmr1* knockout mice with CRISPR–Gold. Our results indicated that CRISPR–Gold has the potential to treat brain disorders that are caused by the overexpression of genes in localized brain regions. We selected *Grm5* as a potential target for CRISPR–Gold-based therapeutic gene editing because a wide number of studies have demonstrated that exaggerated mGluR5 signalling can generate FXS pathophysiology. Therefore, knocking out the mGluR5 gene through nonviral CRISPR gene editing in specific regions of the brain may be a therapeutic way to treat patients with FXS. However, it is unclear whether exaggerated mGluR5 signalling-mediated FXS phenotypes are caused by focal overactivation of (versus global) mGluR5 signalling, and, if so, which parts of the brain need to have the mGluR5 gene deleted to ameliorate the specific behavioural phenotypes. Furthermore, the delivery challenges associated with gene editing in the brain with Cas9 RNPs need to be solved to be used as treatments of brain disorders. To address these two unresolved issues in therapeutic brain gene editing, we generated CRISPR–Gold Cas9 sgRNA RNPs targeting *Grm5*, and investigated their ability to knockout the mGluR5 gene in vivo and rescue mice from the behavioural phenotypes of FXS using *Fmr1* knockout mice, a mouse model of FXS. We first confirmed that CRISPR–Gold-mediated mGluR5 gene editing is successful, in vitro and in cells, as shown in Supplementary Fig. 7. We then stereotaxically injected either saline vehicle (control) or CRISPR–Gold targeting the mGluR5 gene (mGluR5–CRISPR) into the striatum of wild-type or *Fmr1* knockout mice to determine whether CRISPR–Gold could knockout the mGluR5 gene in vivo in the striatum after a direct local injection (Fig. 5a). Tracking of indels by decomposition (TIDE) analysis indicated that there was a frequency of 14.6% in mGluR5 gene mutations (Supplementary Fig. 8a), and that there were no significant off-target effects (Supplementary Fig. 8b). As a result, the mRNA levels and the protein levels of mGluR5 were reduced by 40–50% both in wild-type and *Fmr1* knockout mice, which was confirmed by quantitative PCR with reverse transcription (RT–qPCR) (Fig. 5b) and immunostaining analysis (Fig. 5c). Mice treated with mGluR5–CRISPR also had no evidence of an increased immune response, as measured by mRNA levels of microglial markers in mGluR5–CRISPR-treated brains (Supplementary Fig. 9).

Behavioural rescue in *Fmr1* knockout mice by CRISPR–Gold. Commonly known repetitive behaviours of mice with autistic phenotypes include excessive digging behaviour, which can be observed in the marble-burying assay, and increased jumping, which can be

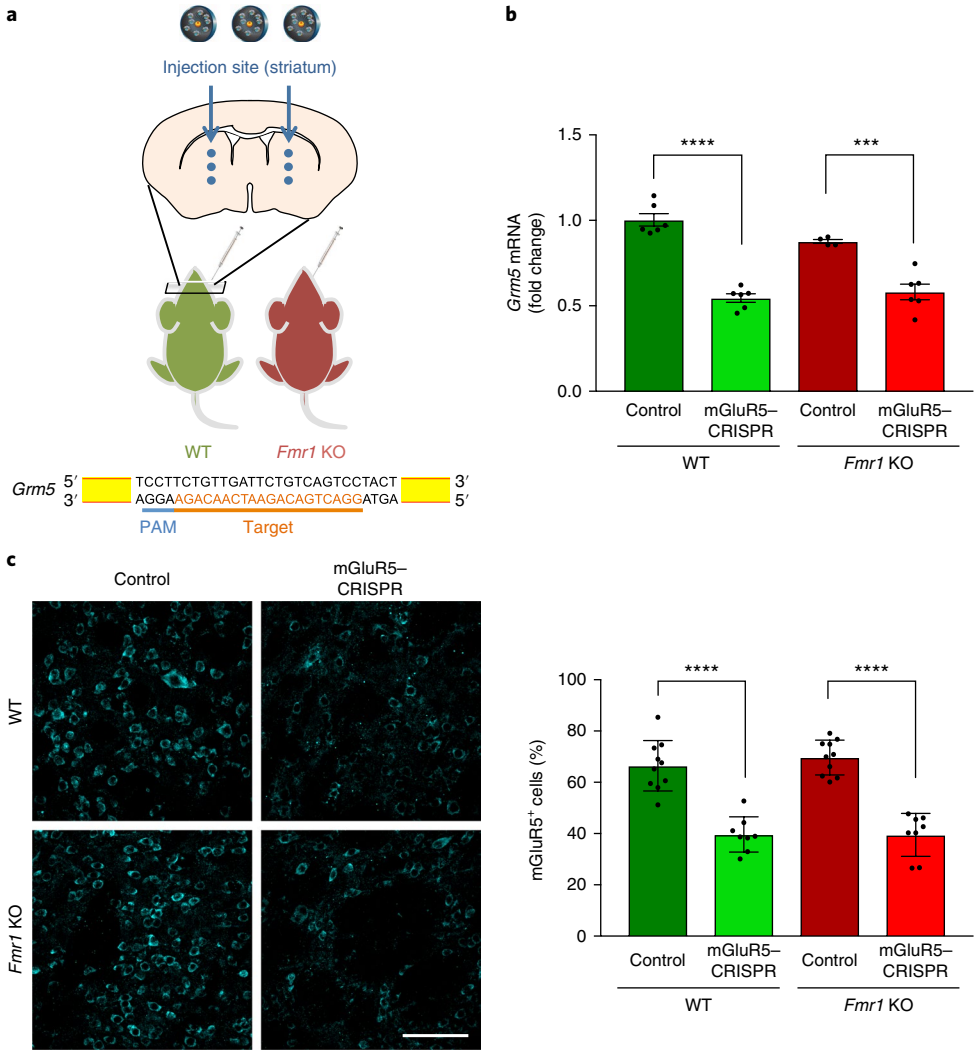

Fig. 5 | mGluR5–CRISPR successfully promotes mGluR5 gene editing in the striatum of wild-type and *Fmr1* knockout mice. a, Upper: schematic of the injection process for mGluR5–CRISPR into the striatum of wild-type (WT) and *Fmr1* knockout (KO) mice. Saline or mGluR5–CRISPR was injected into the striatum (Bregma: 0.26 mm, 3 injection sites per hemisphere are indicated as blue dots, 0.4-mm interval) of WT or *Fmr1* KO mice. Lower: schematic of the target sequences of Cas9 RNPs and the protospacer adjacent motif (PAM) for *Grm5* knockout. **b**, RNA was extracted from the saline-injected control side (control) or from the mGluR5–CRISPR-injected side (mGluR5–CRISPR) of WT or *Fmr1* KO mice 11 weeks after stereotaxic injections. mRNA levels of *Grm5* were amplified and analysed by RT-qPCR. Fold-change of *Grm5* mRNA levels are shown after normalization against *PPIA* mRNA levels. $n = 4$–6, mean ± s.e.m., $^{***}P < 0.001$, $^{****}P < 0.0001$, one-way ANOVA. **c**, Left: immunostaining of mGluR5 (cyan) 5 weeks after stereotaxic injection of saline (control) or mGluR5–CRISPR into the striatum of WT or *Fmr1* KO mice. Scale bar, 100 μm. Right: the number of mGluR5$^+$ cells in WT control, WT mGluR5–CRISPR, *Fmr1* KO control and *Fmr1* KO mGluR5–CRISPR groups were counted and normalized to the number of DAPI$^+$ cells. $n = 8$–10, mean ± s.e.m., $^{****}P < 0.0001$ by one-way ANOVA. *P* values were calculated between WT control and *Fmr1* KO control, WT control and WT mGluR5–CRISPR, or *Fmr1* KO control and *Fmr1* KO mGluR5–CRISPR.

observed during empty cage observations[34]. Given that the striatum is an important brain region in mediating repetitive behaviours[35], we wanted to test whether knocking out the mGluR5 gene by CRISPR–Gold delivery of Cas9 RNPs can rescue the exaggerated repetitive behaviours shown in *Fmr1* knockout mice[36]. Figure 6 shows the effect of injecting saline (control) or mGluR5–CRISPR into the striatum on repetitive behaviours in wild-type and *Fmr1* knockout mice. In the marble-burying assay, *Fmr1* knockout mice injected with saline buried significantly more marbles than wild-type mice. Conversely, injection with mGluR5–CRISPR into the striatum significantly rescued the excessive digging phenotype of *Fmr1* knockout mice back to normal, while having no significant effect on wild-type mice (Fig. 6a, representative movies are shown in Supplementary Video 1). Likewise, the same effect was shown in jumping behaviour in *Fmr1* knockout mice, whereby those injected with mGluR5–CRISPR showed a phenotype much more comparable to wild-type mice compared with *Fmr1* knockout mice injected with saline (Fig. 6b, representative movies are shown in Supplementary Video 2).

To determine whether the rescue of excessive digging and jumping behaviour in *Fmr1* knockout mice were the consequences of potentially reduced hyperlocomotor activities induced by mGluR5–CRISPR, locomotor activities in these mice were also assessed. This behaviour can be assessed via line crossings during empty cage observations[37], the distance that a mouse travels during an open-field activity assay[38], and how long it takes for a mouse to fall in the accelerated rotarod performance test[39]. While there was a significant difference between wild-type and *Fmr1* knockout mice when it

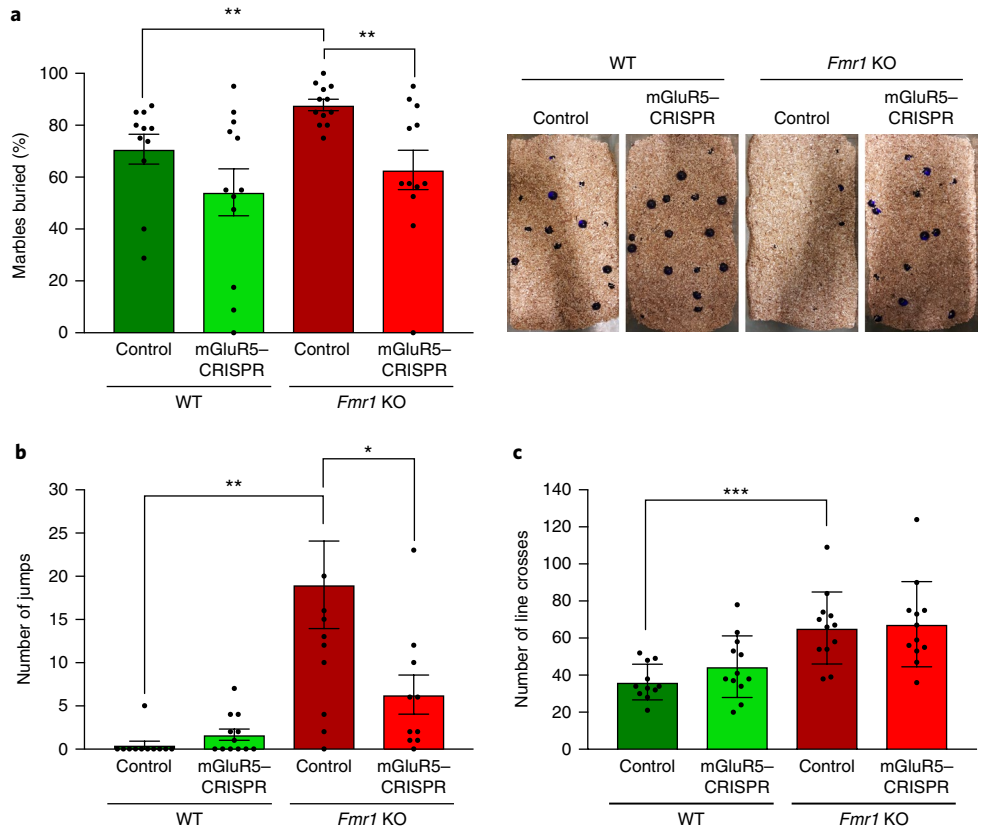

Fig. 6 | Knocking out mGluR5 using mGluR5–CRISPR significantly rescues the increased repetitive behaviours in *Fmr1* knockout mice. a–**c**, Three weeks after stereotaxic injection of either saline (control) or mGluR5–CRISPR into the striatum of WT and *Fmr1* KO mice, the marble-burying assay (**a**) or the empty cage observation test (**b**,**c**) was performed. **a**, Left: percentage of marbles buried after 30 min of the marble-burying test. Right: representative images after marble-burying assay for 30 min. Jumping (**b**) and line crossing behaviours (**c**) were scored during 10 min of an empty cage observation test. $n = 10$–12 for each group, mean ± s.e.m., $^{*}P < 0.05$, $^{**}P < 0.01$, $^{***}P < 0.001$ by one-way ANOVA. *P* values were calculated between WT control and *Fmr1* KO control, WT control and WT mGluR5–CRISPR, or *Fmr1* KO control and *Fmr1* KO mGluR5–CRISPR.

comes to these phenotypes, there was no significant change in locomotor activity in *Fmr1* knockout mice that had been treated with mGluR5–CRISPR. *Fmr1* knockout mice treated with mGluR5–CRISPR performed similarly to control *Fmr1* knockout mice in the three locomotor activity experiments (Fig. 6c and Supplementary Fig. 10), suggesting that exaggerated mGluR5 signalling in the striatum does not mediate the hyperlocomotor activity shown in *Fmr1* knockout mice. In other words, increased repetitive behaviours were specifically rescued by local treatment of mGluR5–CRISPR to the striatum of *Fmr1* knockout mice. Finally, mGluR5–CRISPR-treated *Fmr1* knockout mice had similar body weights to control *Fmr1* knockout mice (Supplementary Fig. 11). Taken together, these results demonstrate that gene editing via the nonviral delivery of CRISPR into a local brain region can rescue specific behavioural phenotypes in an autism mouse model.

Discussion

CRISPR–Gold was able to deliver CRISPR–Cas9 and Cpf1 and edit genes in local regions of the brain after an intracranial injection. Although local gene editing may treat numerous behavioural deficits, gene editing in broad areas of the brain may be necessary for a number of neurological disorders. For these types of brain disorders, alternative strategies for delivering CRISPR–Cas9 will need to be developed, such as convection-enhanced delivery of CRISPR–Cas9 or delivery into the cerebrospinal fluid via intrathecal injection. In addition, CRISPR–Gold has broad cell tropism and can edit multiple cell types in the brain after a local injection. Although targeting diverse cell types other than neurons, including astrocytes and microglia, can be useful (as neurons as well as non-neuronal cells are important targets in numerous diseases), a gene-editing therapy that can target a specific cell type, such as neurons, may be also needed. Finally, as the GNP core of CRISPR–Gold can potentially accumulate in the brain after multiple injections, this may prevent CRISPR–Gold from being injected into patients multiple times. However, a single injection into the brain of an extremely low dose of gold in CRISPR–Gold (2.84 μg kg^{-1}) efficiently rescued behavioural deficits in mice, and appears to be well tolerated in the brain.

Outlook

We have showed that CRISPR–Gold can deliver both Cas9 and Cpf1 RNPs in the brain after an intracranial injection and can edit genes. Currently, gene editing in the adult brain is mainly accomplished through the viral delivery of CRISPR–Cas9[6]. However, there is great interest in developing nonviral methods for delivering RNA-guided endonucleases into the brain due to the potential toxicity caused from using viruses to edit neurons[7–9]. Cas9 RNPs engineered with multiple NLS signals can edit genes in the adult brain when intracranially injected[10]; however, therapeutic gene editing in the brain has still not been accomplished via RNP delivery. CRISPR–Gold-mediated gene editing in adult mouse brains has multiple unique features. CRISPR–Gold was able to edit genes in neurons and in non-neuronal cells important for brain function, including microglia, which have been difficult to edit via other methods, such as viral delivery[40–42]. In addition, CRISPR–Gold was able to inhibit 40–50% of the autism causal gene *Grm5* in the striatum after an intracranial

injection, and this level of inhibition was able to rescue mice from increased repetitive behaviours, which is one of the core symptoms of ASDs. Importantly, CRISPR–Gold-mediated editing was localized to the striatum, suggesting that global inhibition of neuronal signalling pathways is not needed to rescue autism-associated behavioural phenotypes. Taken together, CRISPR–Gold-mediated gene editing of adult mouse brains, via the nonviral delivery of Cas9 RNPs, can rescue mice from behavioural deficits and has the potential to enable the rapid development of focal brain-knockout animal models.

Methods

See Supplementary Tables 1–5 for additional information.

Materials. Oligonucleotides were purchased from Integrated DNA Technologies. GNPs (60 nm) were purchased from BBI Solutions. Sodium citrate and HEPES were purchased from Mandel Scientific. Sodium silicate was purchased from Sigma-Aldrich. Phusion High-Fidelity DNA Polymerase was purchased from NEB. The MEGAscript T7 kit, the MEGAclear kit, the PageBlue solution, the propidium iodide and the PureLink Genomic DNA kit were purchased from ThermoFisher. Mini-PROTEAN TGX Gels (4–20%) were purchased from Bio-Rad. DMEM media, non-essential amino acids, penicillin–streptomycin, Dulbecco's PBS and 0.05% trypsin were purchased from Life Technologies. Amicon Ultra-4 30 kDa was purchased from EMD Millipore. Cas9 proteins with an amino-terminal 6xHis-tag and two SV40 NLS peptides at the carboxyl terminus and Cpf1 proteins were purchased from Macrolab UC Berkeley. The Poly (PAsp(DET)) was a gift from Kazunori Kataoka's group[43,44]. The SYTOX Red Dead Cell Stain (excitation/emission of 640/658 nm) and the SuperScript III First-Strand Synthesis kit were purchased from Invitrogen.

Antibodies. The mouse monoclonal RFP antibody (6G6) was purchased from ChromoTek, the chicken polyclonal GFP antibody (GFP-1020) from Aves Labs (Tigard), the rabbit polyclonal GFAP antibody (AB5804) and the mouse monoclonal NeuN antibody (MAB377) from Millipore, the rabbit polyclonal IBA1 antibody (019-19741) from Wako Chemicals, and the rabbit polyclonal mGluR5 antibody (AGC-007) was from Alomone Labs. The goat anti-mouse IgG2a-Cy3, goat anti-chicken-Cy2, goat anti-rabbit-Cy5, goat anti-mouse IgG1-Cy5 and donkey anti-rabbit IgG-Alexa Fluor 647 antibodies were purchased from Jackson ImmunoResearch Laboratories.

In vitro T7 transcription of sgRNA and crRNA. The DNA templates for the in vitro transcription of sgRNAs and crRNAs (sgRNAs for Cas9 and crRNAs for Cpf1) were prepared by PCR. Sequences of the template and primers are listed in Supplementary Tables 1 and 2. Two sequences (left and right) of guide RNAs were used for the Ai9-targeting experiments. A single sequence for sgRNAs and crRNAs for targeting the YFP gene (*yfp*) and sgRNAs for targeting *Grm5* was used. PCR amplification was performed with Phusion Polymerase according to the manufacturer's protocol. RNA in vitro transcription was performed using the MEGAscript T7 kit, and purification of the resulting RNA was conducted using the MEGAclear kit following the manufacturer's protocol. The transcribed sgRNAs and crRNAs were eluted into 20 mM HEPES buffer. The concentration of RNAs was determined using a Nanodrop 2000 spectrophotometer, and the final guide RNA products were stored at −80 °C for subsequent experiments. Ai9 sgRNA target sequences were chosen as previously described[45] and other target sequences were designed in-house.

Synthesis of CRISPR–Gold. GNPs (60 nm in diameter, 450 nM) were reacted with a 5′ thiol-modified single stranded oligonucleotide (DNA-SH), 26 bases in length (/5ThioMC6-D/GAAATATGCCAGAAATATCTGTCAGA, 200 μM), which had no sequence specificity. The reaction was performed in an Eppendorf tube in nuclease-free water (160 μl). A 100 mM sodium citrate solution (pH 3.5, 40 μl) was added to the reaction, and the reaction was allowed to proceed overnight[46]. Unconjugated DNA-SH was removed by centrifugation at 3,000*g* for 10 min, and was washed two times with 20 mM HEPES buffer. The GNP–DNA solution was stored at 4 °C until further use. CRISPR–Gold was synthesized using a layer-by-layer method. Cas9 or Cpf1 (50 pmole in 10 μl) and guide RNAs (50 pmole guide RNA in 10 μl) were mixed in 80 μl of Cas9 or Cpf1 buffer (50 mM HEPES (pH 7.5), 300 mM NaCl and 10% (vol./vol.) glycerol) for 5 min at room temperature, and this solution was then added to the GNP–DNA solution (0.45 pmole of GNPs), generating GNP–Cas9 or Cpf1 RNP. Freshly diluted sodium silicate (6 mM, 2 μl) was added to the GNP–Cas9 RNP solution and incubated for 5 min at room temperature. The mixture was then centrifuged using an EMD Millipore Amicon Ultra-4 30 kDa at 2,000*g* for 5 min to remove unbound molecules. The recovered GNP–Cas9 RNP–silicate was mixed with 5 μg of PAsp(DET) solution and incubated for 5 min at room temperature to form the last layer of CRISPR–Gold immediately before treatment.

Gel electrophoresis to measure Cas9 and Cpf1 RNP loading in CRISPR–Gold. Strong non-covalent interactions allow the interaction of GNP–DNA with Cas9 and Cpf1 RNPs. Gel analysis was conducted to visualize Cas9 and Cpf1 RNP loading on CRISPR–Gold. CRISPR–Gold was synthesized using the above-described method with Cas9, sgRNA_Ai9_L, sgRNA_Ai9_R, and Cpf1 and crRNA_*yfp*. The synthesized CRISPR–Gold was purified using a Vivaspin 300 kDa concentrator at 2,000*g* for 5 min to remove unbound molecules, and then one step of washing was conducted. Each sample collected before and after the purification step was analysed by gel electrophoresis using a 4–20% Mini-PROTEAN TGX Gel, stained with SYBR Green (ThermoFisher). Additionally, the same gel was stained with Coomassie Blue to visualize the Cas9 and Cpf1 proteins. Images were taken with ChemiDoc MP using the ImageLab software (Bio-Rad).

Animal care and use. Ai9 (in C57BL/6J background), Thy1-YFP (in C57BL/6J background), *mdx*, wild-type (in FVB background: FVB.129P2-*Pde6b*$^{+}$ *Tyr*$^{c\text{-}ch}$/AntJ) and *Fmr1* knockout (in FVB background: FVB.129P2-*Pde6b*$^{+}$ *Tyr*$^{c\text{-}ch}$ *Fmr1*^{tm1Cgr}/J) mice were obtained from The Jackson Laboratory. The use and care of animals in this study followed the guidelines of the UTHSCSA and UC Berkeley Institutional Animal Care and Use Committee.

Primary culture of hippocampal neurons from wild-type FVB mice. Hippocampal neurons isolated from embryonic day 17 mouse brains (wild-type FVB mice) were plated at a density of 1–3 × 10^5 cells per well as described previously[47]. Cells were kept at 37 °C in a humidified, CO_2-controlled (5%) incubator. Primary cultured hippocampal neurons were cultured for 7 days and were treated with either neurobasal medium only or CRISPR–Gold complexes including RNPs (25 pmole of Cas9 or 25 pmole of sgRNAs) with 2.5 μg of PAsp(DET) added in the neurobasal medium to test for electrophysiological properties and toxicity. Fourteen days after CRISPR–Gold treatment, the cells were stained with SYTOX Red and fixed with 4% paraformaldehyde, followed by phalloidin-Alexa488 staining with DAPI.

Whole-cell recording. After 10–14 days of CRISPR–Gold treatment, primary cultured hippocampal neurons were patched and recorded. The extracellular solution contained NaCl (124 mM), KCl (2 mM), $MgSO_4$ (2 mM), NaH_2PO_4 (1.25 mM), $CaCl_2$ (2 mM), $NaHCO_3$ (26 mM), D-dextrose (10 mM) and vitamin C (0.4 mM). The recordings were conducted at room temperature with an internal solution of potassium gluconate (120 mM), KCl (20 mM), $MgCl_2$ (2 mM), HEPES (10 mM), ATP (2 mM), GTP (0.25 mM) and EGTA (0.1 mM, pH 7.4). Pyramidal cells were identified at ×60 magnification using a water-submersible objective and differential interference contrast/infrared optics on a BX51WI Olympus microscope. Recordings were conducted at 25 °C. Voltage recordings were performed using bridge balance compensation via the amplifier (HEKA, EPC10). If slow capacitance changed by more than 20% during recordings, the cell was excluded from further analysis. A hardware filter of 3 kHz was used for data collection. Input resistance was measured using a −20 pA current injection from the resting voltage. Action potentials were evoked from a holding current to maintain −80 mV, and spikes were generated by rectangular current injection (1 s duration, 200 pA). Action potential frequency was measured 3 min after break-in into the whole cell.

Culture of YFP-expressing HEK cells. YFP-HEK cells were generated by infection of HEK293T cells (from the Cell Culture Facility at UC Berkeley, authenticated using short tandem repeat (STR) profiling) with a YFP-containing lentivirus, and clonal selection was performed for cells expressing YFP. YFP-HEK cells were cultured in the culture medium (DMEM with 10% FBS, 1× MEM, non-essential amino acids and 100 μg ml^{-1} penicillin–streptomycin). The cells were tested for mycoplasma contamination and the result was negative. Nucleofection was conducted on the YFP-HEK cells.

Primary culture of fibroblasts from Ai9 mice. Primary fibroblasts were obtained from the muscles of Ai9 mice. Collagenase-treated tissues were minced with scaffold and digested in a collagenase and trypsin mixture[48]. The cells were plated in 10-cm culture dishes with the culture medium. Cells that were not firmly attached were removed during media changes that were conducted every 24 h. Fibroblasts were passaged with Accutase, and transfection with Cas9 or Cpf1 was conducted with fibroblasts within 14 days of culture.

Nucleofection. Cells were detached using Accutase, spun down at 600 *g* for 3 min and washed with PBS. Nucleofection was conducted using an Amaxa 96-well Shuttle system following the manufacturer's protocol using 10 μl of Cas9 RNPs (100 pmole of Cas9, 120 pmole of guide RNAs) or Cpf1 RNPs (100 pmole of Cpf1, 120 pmole of crRNAs)[49]. Cells (10^5) were transfected using the EH-100 Lonza program. After nucleofection, medium (500 μl) was added and the cells were incubated at 37 °C in tissue culture plates. The cell culture medium was changed the next day, and the cells were then incubated for 7 days before flow cytometry analysis.

Flow cytometry analysis fluorescence microscopy. Flow cytometry was used to quantify the expression levels of YFP in YFP-HEK cells or the expression levels of tdTomato in primary Ai9 fibroblasts after transfecting with Cas9 or Cpf1.

The cells were analysed 7 days after transfection. The cells were washed with PBS and detached using Accutase. YFP and tdTomato expression was quantified using BD LSR Fortessa X-20 and Guava easyCyte, and analysis was conducted with FlowJo.

In vitro and in-cell cleavage assays. The mGluR5 template was PCR amplified (mGluR5 forward: CCTTAATGCACCACTCAGCA, mGluR5 reverse: GGCTTCCACTCTCTGAATGC) from mouse genomic DNA. For in vitro cleavage assays, the template DNA was incubated with *Grm5* sgRNA and Cas9 proteins (*Grm5* Cas9 RNPs) in a 1.5-ml tube. Gel electrophoresis was performed to verify cleavage of the template. For cleavage assays in the myoblasts from *mdx* mice, *Grm5* Cas9 RNPs were introduced into the cell by electroporation. The mGluR5 gene was then PCR amplified from the myoblast, and a surveyor assay was conducted to check targeted gene editing.

Stereotaxic injection of CRISPR–Gold into the mouse brain. Mice (1–2 months old) were anaesthetized via an intraperitoneal injection of 100 mg kg^{-1} ketamine and 10 mg kg^{-1} xylazine. Preemptive analgaesia was given (Buprenex, 1 mg kg^{-1}, intraperitoneally). Craniotomy was performed according to approved procedures, and 2 µl of CRISPR–Gold (50 pmole of Cas9 and 50 pmoles of guide RNAs, or 50 pmole of Cpf1 and 50 pmole of crRNAs) with 5 µg of PAsp(DET) for Thy1-YFP or Ai9 mice was injected into a single hemisphere of the striatum and/or the dorsal dentate gyrus of the hippocampus. The uninjected contralateral side was used as a control. For stereotaxic injection with mGluR5–CRISPR, 2 µl of saline (control) or CRISPR–Gold loaded with Cas9–mGluR5 RNPs (50 pmole of Cas9 and 50 pmole of sgRNAs) was injected into the striatum of both hemispheres of wild-type or *Fmr1* knockout mice. Injection was given separately into three spots in each hemisphere with a 0.4 mm interval. The incision was clipped and proper post-operative analgaesics were administered for 6 days following surgery.

Deep sequencing analysis of CRISPR–Gold-treated brain tissue. The target sequences of the genomic region were amplified by PCR using Phusion High-Fidelity Polymerase according to the manufacturer's protocol. Target genes were amplified first with primer sets and then amplified again with the deep sequencing primers listed in Supplementary Table 3. Barcode primers were designed as previously described[50]. The amplicons were purified using the ChargeSwitch PCR clean-up kit (ThermoFisher). PCR with barcode primers was conducted to attach Illumina adapters for deep sequencing. PCR clean-up was performed an additional time. The Berkeley Sequencing facility performed DNA quantification using a Qubit 2.0 Fluorometer (Life Technologies). BioAnalyzer for size analysis and qPCR quantification followed. The library was sequenced using the Illumina HiSeq2500 in the Vincent Coates Genomic Sequencing Laboratory at UC Berkeley. The analysis was conducted using the CRISPR Genome Analyzer[51].

TIDE assay. The mGluR5 target gene was amplified by PCR using Phusion Polymerase. The PCR amplicon was sent to Quintara Bioscience for sequencing. The sequencing result was analysed with TIDE software to quantify indel mutation efficiency (https://tide-calculator.nki.nl/)[52].

Off-target analysis. Off-target prediction was conducted using Cas9-OFFinder (http://www.rgenome.net/cas-offinder/). Only the top two off-target sites had more than ten base matches. Genomic DNA extracted from mouse brains that were injected with mGluR5–CRISPR (CRISPR–Gold complex) was used to amplify two off-target sites. A surveyor assay and polyacrylamide gel electrophoresis were conducted to detect cleaved products.

RNA extraction from mouse brains and RT–qPCR. Mice were perfused with ice-cold PBS at 11 weeks after injection. Brains were cut into 1-mm sections using a brain slicer matrix (Zivic Instrument) around the injection sites. The brain slices were washed with ice-cold PBS and the injection region (1-mm thick, ~2-mm wide, ~2-mm long) was cut out. After adding TRIzol (800 µl), the brain slices were homogenized, treated with chloroform (160 µl) and centrifuged for 15 min at 4 °C. The aqueous phase of the sample was removed by pipet and 100% isopropanol (400 µl) was added. After being centrifuged for 10 min, the supernatant was removed from the tube, and the pellet was washed with 75% ethanol and centrifuged for 5 min. Afterwards, the supernatant was removed and the pellet was dissolved in DNase- and RNase-free water. RNA (1 µg) was reverse-transcribed using the SuperScript III First-Strand Synthesis kit. RT–qPCR analysis was performed using PowerUp SYBR Green Master Mix (Applied Biosystems) with the primers listed in Supplementary Table 4. The relative expression from RNA samples was analysed using the $2^{-\Delta\Delta CT}$ method. Values were normalized against the gene expression of the housekeeping gene *PPIA*.

Immunostaining. Two weeks after stereotaxic injection of 1–2-month-old adult mice, the mice were anaesthetized by isoflurane and the left ventricle perfused with ice-cold PBS followed by 4% paraformaldehyde in PBS. The brains were post-fixed for 4 h in 4% paraformaldehyde, washed once with PBS and then transferred to 30% sucrose in PBS at 4 °C. Hippocampal sections from the mice were obtained by cryostat (CM3050S; Leica Microsystems). Before sectioning, brains were cryoprotected by incubating in 30% sucrose, embedded in O.C.T. compound, frozen and then stored at −80 °C until slicing. Slices were cut on the coronal plane at 20 µm, mounted on glass slides and stored at 4 °C. The sections to be immunostained were washed three times in PBS. Antigen retrieval was performed by steaming in a citrate buffer (0.294% sodium citrate, 0.05% Tween 20 in distilled water, pH 6.0) for 15 min with subsequent cooling over ice for 10 min. The sections were rinsed in PBS and blocked (5% goat serum, 0.2% Triton X-100 in PBS) overnight at 4 °C. The sections were incubated in the same blocking solution with primary antibodies at room temperature for 1 h. The sections were washed in PBS before incubation with secondary antibodies for 2 h. After rinsing once more in PBS, the sections were mounted in Prolong Gold Antifade Reagent with DAPI and imaged using a Zeiss confocal microscope.

Analysis and statistics for immunostaining. Quantification of fluorescence was performed on images taken with the same exposure times and within the same experiment. To determine relative YFP intensities in Thy1-YFP mice, a defined region of interest (ROI), which was the same size for all images analysed, was traced in the hippocampus using Image J software (NIH). To quantify YFP gene knockdown, YFP$^+$ cells were also counted and normalized to DAPI$^+$ cells in a defined ROI. To determine the percentage of edited cells or to present the number of DAPI$^+$ cells in Ai9 mice, tdTomato$^+$ cells were counted and normalized against the number of DAPI$^+$ cells or the number of DAPI$^+$ cells were presented itself (analysed from a defined ROI, which was the same size for all images analysed for comparison). To determine the percentage of cell types among edited cells, GFAP$^+$, IBA1$^+$ or NeuN$^+$ cells were counted in only tdTomato$^+$ cells. The percentage of the tdTomato$^+$ cells among the cell types was also analysed by counting GFAP$^+$, IBA1$^+$ or NeuN$^+$ cells co-stained with tdTomato among the total GFAP$^+$, IBA1$^+$ or NeuN$^+$ cells. Each cell marker was stained with tdTomato and analysed independently. To compare the uninjected group and the injected group, Student's unpaired *t*-test (two-tailed) was used. For mGluR5 immunostaining analysis, the number of mGluR5 immunofluorescent$^+$ cells was quantified by using a minimum intensity threshold of 110 (range 0 to 255) using Image J software. The mGluR5$^+$ cells were normalized to all DAPI$^+$ cells in the field. Images were quantified from each brain hemisphere (two images per brain), corresponding to the control or CRISPR–Gold-injected hemispheres. The size of the brain region quantified was 212.55 µm^2 around the injection site, in either the control-injected striatum or the CRISPR–Gold-injected striatum (~200 cells were counted). One-way analysis of variance (ANOVA) was used for the statistical analysis. All the statistics showed that variances are similar between the groups that are being statistically compared. No statistical methods were used to pre-determine sample sizes, but all sample sizes are similar to those generally employed in the field. Sample size (n) is indicated in each figure legend. The injection side was randomized (left or right side of the brain) for each experiment.

Behavioural test sequence and statistics. Behavioural tests were performed on mice at 2 weeks post-injection in the following order: empty cage observations, marble-burying assay, open-field activity assay, and rotarod performance test, followed by weighing and perfusion of all animals (Supplementary Table 5). A total of 47 mice ($n = 11$–12 per group) were used as a cohort. Identification of each animal was determined after testing to ensure that the experimenter remained blinded to the genotype or treatment of the test subject. Unless otherwise noted, data were analysed by one-way ANOVA using GraphPad Prism7 software.

Empty cage observations. The test was performed as previously described[53] with minor modifications. The mice were brought into a testing room with normal lighting 1.5 h before testing, after which they were individually placed in a test cage identical to their home cage (30-cm wide, 19-cm long, 13-cm high) without bedding to prevent digging for 10 min of habituation. Videotaping of the cage was recorded using a DV Cam camera for 12 min while the mouse was allowed to freely explore. The last 10 min of the video was analysed by investigators who were blinded to the genotype or treatment of the test subject for line-crossing (crossing an imaginary line at the centre of the cage) and jumping behaviours.

Marble-burying assay. The test was performed as previously described[36,54] with minor modifications to evaluate repetitive digging behaviour. The mice were brought into the testing room with normal lighting 1.5 h before testing, after which they were individually placed in a cage identical to the test cage (30-cm wide, 19-cm long, 13-cm high) for 30 min of habituation. The test cage was filled with 3 cm of Teklad Sani-Chip bedding, and 20 dark blue marbles (15 mm diameter) were placed in a 5 × 4 pattern equidistant to each other and the side of the cage. The mice were then placed into the test cage and allowed to freely explore for 30 min. A marble was considered buried if two-thirds of the marble's surface was covered by bedding. The percentage of marbles buried was then scored by four different investigators who were blinded to the genotype or treatment of the test subject.

Open-field activity assay. The open-field activity assay was performed as previously described[36] with minor modifications. The mice were brought into the dark testing room with dim red lighting 1 h before the test, after which they were

individually placed in a cage identical to their home cage for 30 min. The mice were then placed in the right corner of a clear acrylic chamber and allowed to freely explore for 30 min. Specific parameters, such as total distance travelled for 30 min, were measured to determine motor activity.

Rotarod performance test. The rotarod apparatus was used to measure locomotor activity[36]. During the training period, mice were allowed to explore the cylinder of the rotarod for 2 min with constant rotation at a speed of 4 r.p.m. After 5 min of rest, they were put on the rotarod and the speed was accelerated to 4–40 r.p.m. over a period of 300 s. The latency to fall off the rotarod within this time period was recorded (up to 300 s). Mice underwent four trials, and the mean latency to fall off the rotarod for all four trials was combined and calculated.

Reporting Summary. Further information on experimental design is available in the Nature Research Reporting Summary linked to this article.

Data availability. The authors declare that all data supporting the findings of this study are available within the paper and its Supplementary Information.

Received: 15 December 2016; Accepted: 16 May 2018;
Published online: 25 June 2018

References

1. Jinek, M. et al. A programmable dual-RNA-guided DNA endonuclease in adaptive bacterial immunity. *Science* **337**, 816–821 (2012).
2. Cong, L. et al. Multiplex genome engineering using CRISPR/Cas systems. *Science* **339**, 819–823 (2013).
3. Mali, P. et al. RNA-guided human genome engineering via Cas9. *Science* **339**, 823–826 (2013).
4. Cho, S. W., Kim, S., Kim, J. M. & Kim, J. S. Targeted genome engineering in human cells with the Cas9 RNA-guided endonuclease. *Nat. Biotechnol.* **31**, 230–232 (2013).
5. Zetsche, B. et al. Cpf1 is a single RNA-guided endonuclease of a class 2 CRISPR–Cas system. *Cell* **163**, 759–771 (2015).
6. Swiech, L. et al. In vivo interrogation of gene function in the mammalian brain using CRISPR–Cas9. *Nat. Biotechnol.* **33**, 102–106 (2015).
7. Mingozzi, F. & High, K. A. Immune responses to AAV vectors: overcoming barriers to successful gene therapy. *Blood* **122**, 23–36 (2013).
8. Ishida, K., Gee, P. & Hotta, A. Minimizing off-target mutagenesis risks caused by programmable nucleases. *Int. J. Mol. Sci.* **16**, 24751–24771 (2015).
9. Watakabe, A. et al. Comparative analyses of adeno-associated viral vector serotypes 1, 2, 5, 8 and 9 in marmoset, mouse and macaque cerebral cortex. *Neurosci. Res.* **93**, 144–157 (2015).
10. Staahl, B. T. et al. Efficient genome editing in the mouse brain by local delivery of engineered Cas9 ribonucleoprotein complexes. *Nat. Biotechnol.* **35**, 431–434 (2017).
11. Kazdoba, T. M., Leach, P. T., Silverman, J. L. & Crawley, J. N. Modeling fragile X syndrome in the Fmr1 knockout mouse. *Intractable Rare Dis. Res.* **3**, 118–133 (2014).
12. Persico, A. M. & Napolioni, V. Autism genetics. *Behav. Brain Res.* **251**, 95–112 (2013).
13. Ji, N. Y. & Findling, R. L. Pharmacotherapy for mental health problems in people with intellectual disability. *Curr. Opin. Psychiatry* **29**, 103–125 (2016).
14. Politte, L. C., Henry, C. A. & McDougle, C. J. Psychopharmacological interventions in autism spectrum disorder. *Harv. Rev. Psychiatry* **22**, 76–92 (2014).
15. Bear, M. F., Huber, K. M. & Warren, S. T. The mGluR theory of fragile X mental retardation. *Trends Neurosci.* **27**, 370–377 (2004).
16. Bear, M. F. Therapeutic implications of the mGluR theory of fragile X mental retardation. *Genes Brain Behav.* **4**, 393–398 (2005).
17. Dölen, G. & Bear, M. F. Role for metabotropic glutamate receptor 5 (mGluR5) in the pathogenesis of fragile X syndrome. *J. Physiol.* **586**, 1503–1508 (2008).
18. Osterweil, E. K., Krueger, D. D., Reinhold, K. & Bear, M. F. Hypersensitivity to mGluR5 and ERK1/2 leads to excessive protein synthesis in the hippocampus of a mouse model of fragile X syndrome. *J. Neurosci.* **30**, 15616–15627 (2010).
19. Tao, J. et al. Negative allosteric modulation of mGluR5 partially corrects pathophysiology in a mouse model of Rett syndrome. *J. Neurosci.* **36**, 11946–11958 (2016).
20. Silverman, J. L. et al. Negative allosteric modulation of the mGluR5 receptor reduces repetitive behaviors and rescues social deficits in mouse models of autism. *Sci. Transl. Med.* **4**, 131ra151 (2012).
21. Jacquemont, S. et al. Epigenetic modification of the FMR1 gene in fragile X syndrome is associated with differential response to the mGluR5 antagonist AFQ056. *Sci. Transl. Med.* **3**, 64ra61 (2011).
22. Raspa, M., Wheeler, A. C. & Riley, C. Public health literature review of fragile X syndrome. *Pediatrics* **139**, S153–S171 (2017).
23. Lee, K. et al. Nanoparticle delivery of Cas9 ribonucleoprotein and donor DNA in vivo induces homology-directed DNA repair. *Nat. Biomed. Eng.* **1**, 889–901 (2017).
24. Feng, G. et al. Imaging neuronal subsets in transgenic mice expressing multiple spectral variants of GFP. *Neuron* **28**, 41–51 (2000).
25. Choi, G. B. et al. Driving opposing behaviors with ensembles of piriform neurons. *Cell* **146**, 1004–1015 (2011).
26. Fried, I., Mukamel, R. & Kreiman, G. Internally generated preactivation of single neurons in human medial frontal cortex predicts volition. *Neuron* **69**, 548–562 (2011).
27. McMahon, M. A. & Cleveland, D. W. Gene therapy: gene-editing therapy for neurological disease. *Nat. Rev. Neurol.* **13**, 7–9 (2017).
28. Xie, N. et al. Reactivation of FMR1 by CRISPR/Cas9-mediated deletion of the expanded CGG-repeat of the fragile X chromosome. *PLoS ONE* **11**, e0165499 (2016).
29. Park, C. Y. et al. Reversion of FMR1 methylation and silencing by editing the triplet Repeats in fragile X iPSC-derived neurons. *Cell Rep.* **13**, 234–241 (2015).
30. Madisen, L. et al. A robust and high-throughput Cre reporting and characterization system for the whole mouse brain. *Nat. Neurosci.* **13**, 133–140 (2010).
31. Chen, Y. S. et al. Size-dependent impairment of cognition in mice caused by the injection of gold nanoparticles. *Nanotechnology* **21**, 485102 (2010).
32. Ferreira, G. K. et al. Effect of acute and long-term administration of gold nanoparticles on biochemical parameters in rat brain. *Mater. Sci. Eng. C Mater. Biol. Appl.* **79**, 748–755 (2017).
33. Almad, A. A. & Maragakis, N. J. Glia: an emerging target for neurological disease therapy. *Stem Cell Res. Ther.* **3**, 37 (2012).
34. Sukoff Rizzo, S. J. & Crawley, J. N. Behavioral phenotyping assays for genetic mouse models of neurodevelopmental, neurodegenerative, and psychiatric disorders. *Annu. Rev. Anim. Biosci.* **5**, 371–389 (2017).
35. Kim, H., Lim, C. S. & Kaang, B. K. Neuronal mechanisms and circuits underlying repetitive behaviors in mouse models of autism spectrum disorder. *Behav. Brain Funct.* **12**, 3 (2016).
36. Spencer, C. M. et al. Modifying behavioral phenotypes in Fmr1 KO mice: genetic background differences reveal autistic-like responses. *Autism Res.* **4**, 40–56 (2011).
37. Sungur, A., Vörckel, K. J., Schwarting, R. K. & Wöhr, M. Repetitive behaviors in the Shank1 knockout mouse model for autism spectrum disorder: developmental aspects and effects of social context. *J. Neurosci. Methods* **234**, 92–100 (2014).
38. Ding, Q., Sethna, F. & Wang, H. Behavioral analysis of male and female Fmr1 knockout mice on C57BL/6 background. *Behav. Brain Res.* **271**, 72–78 (2014).
39. Graham, D. R. & Sidhu, A. Mice expressing the A53T mutant form of human alpha-synuclein exhibit hyperactivity and reduced anxiety-like behavior. *J. Neurosci. Res.* **88**, 1777–1783 (2010).
40. Masuda, T., Tsuda, M., Tozaki-Saitoh, H. & Inoue, K. Lentiviral transduction of cultured microglia. *Methods Mol. Biol.* **1041**, 63–67 (2013).
41. Balcaitis, S., Weinstein, J. R., Li, S., Chamberlain, J. S. & Möller, T. Lentiviral transduction of microglial cells. *Glia.* **50**, 48–55 (2005).
42. Burke, B., Sumner, S., Maitland, N. & Lewis, C. E. Macrophages in gene therapy: cellular delivery vehicles and in vivo targets. *J. Leukoc. Biol.* **72**, 417–428 (2002).
43. Kim, H. J. et al. Introduction of stearoyl moieties into a biocompatible cationic polyaspartamide derivative, PAsp(DET), with endosomal escaping function for enhanced siRNA-mediated gene knockdown. *J. Control. Release* **145**, 141–148 (2010).
44. Miyata, K. et al. Polyplexes from poly(aspartamide) bearing 1,2-diaminoethane side chains induce pH-selective, endosomal membrane destabilization with amplified transfection and negligible cytotoxicity. *J. Am. Chem. Soc.* **130**, 16287–16294 (2008).
45. Tabebordbar, M. et al. In vivo gene editing in dystrophic mouse muscle and muscle stem cells. *Science* **351**, 407–411 (2016).
46. Zhang, X., Servos, M. R. & Liu, J. Instantaneous and quantitative functionalization of gold nanoparticles with thiolated DNA using a pH-assisted and surfactant-free route. *J. Am. Chem. Soc.* **134**, 7266–7269 (2012).
47. Lee, H. Y. et al. Bidirectional regulation of dendritic voltage-gated potassium channels by the fragile X mental retardation protein. *Neuron* **72**, 630–642 (2011).
48. Khan, M. & Gasser, S. Generating primary fibroblast cultures from mouse ear and tail tissues. *J. Vis. Exp.* **107**, 53565 (2016).
49. Lin, S., Staahl, B. T., Alla, R. K. & Doudna, J. A. Enhanced homology-directed human genome engineering by controlled timing of CRISPR/Cas9 delivery. *elife* **3**, e04766 (2014).
50. Sanjana, N. E., Shalem, O. & Zhang, F. Improved vectors and genome-wide libraries for CRISPR screening. *Nat. Methods* **11**, 783–784 (2014).

51. Güuell, M., Yang, L. & Church, G. M. Genome editing assessment using CRISPR Genome Analyzer (CRISPR-GA). *Bioinformatics* **30**, 2968–2970 (2014).
52. Brinkman, E. K., Chen, T., Amendola, M. & van Steensel, B. Easy quantitative assessment of genome editing by sequence trace decomposition. *Nucleic Acids Res.* **42**, e168 (2014).
53. McFarlane, H. G. et al. Autism-like behavioral phenotypes in BTBR T+tf/J mice. *Genes Brain Behav.* **7**, 152–163 (2008).
54. Thomas, A. et al. Marble burying reflects a repetitive and perseverative behavior more than novelty-induced anxiety. *Psychopharmacology* **204**, 361–373 (2009).

Acknowledgements

We thank J. Doudna for advice, B. Staahl for discussions and technical support, and H. Kim, A. Rao and K. Kataoka for technical support. We thank M. A. Bhat and members of the Bhat Lab for technical support. We thank M. West in the CIRM/QB3 Shared Stem Cell facility for technical support. This work was supported by the National Institutes of Health grant R01EB023776 to N.M, and by the National Science Foundation grant 1456862 to R.B.

Author contributions

B.L., K.L., R.B., N.M. and H.Y.L. designed the research, and B.L., K.L., S.P., R.G.-R., A.C., H.M.P., V.B. and H.Y.L. performed the experiments and analyses. R.G.-R. and S.P. generated the videos. B.L., K.L., N.M. and H.Y.L. wrote the manuscript. H.Y.L. supervised the research. All authors discussed the results and commented on the manuscript.

Competing interests

K.L., H.M.P. and N.M. are co-founders of GenEdit Inc. The remaining authors declare no competing interests.

Additional information

Supplementary information is available for this paper at https://doi.org/10.1038/s41551-018-0252-8.

Reprints and permissions information is available at www.nature.com/reprints.

Correspondence and requests for materials should be addressed to N.M. or H.Y.L.

Publisher's note: Springer Nature remains neutral with regard to jurisdictional claims in published maps and institutional affiliations.

nature research

Corresponding author(s): Hye Young Lee and Niren Murthy

Reporting Summary

Nature Research wishes to improve the reproducibility of the work that we publish. This form provides structure for consistency and transparency in reporting. For further information on Nature Research policies, see Authors & Referees and the Editorial Policy Checklist.

Statistical parameters

When statistical analyses are reported, confirm that the following items are present in the relevant location (e.g. figure legend, table legend, main text, or Methods section).

n/a	Confirmed	
☒	☐	The exact sample size (*n*) for each experimental group/condition, given as a discrete number and unit of measurement
☐	☒	An indication of whether measurements were taken from distinct samples or whether the same sample was measured repeatedly
☐	☒	The statistical test(s) used AND whether they are one- or two-sided *Only common tests should be described solely by name; describe more complex techniques in the Methods section.*
☐	☒	A description of all covariates tested
☐	☒	A description of any assumptions or corrections, such as tests of normality and adjustment for multiple comparisons
☐	☒	A full description of the statistics including central tendency (e.g. means) or other basic estimates (e.g. regression coefficient) AND variation (e.g. standard deviation) or associated estimates of uncertainty (e.g. confidence intervals)
☐	☒	For null hypothesis testing, the test statistic (e.g. *F*, *t*, *r*) with confidence intervals, effect sizes, degrees of freedom and *P* value noted *Give P values as exact values whenever suitable.*
☒	☐	For Bayesian analysis, information on the choice of priors and Markov chain Monte Carlo settings
☐	☒	For hierarchical and complex designs, identification of the appropriate level for tests and full reporting of outcomes
☒	☐	Estimates of effect sizes (e.g. Cohen's *d*, Pearson's *r*), indicating how they were calculated
☐	☒	Clearly defined error bars *State explicitly what error bars represent (e.g. SD, SE, CI)*

Our web collection on statistics for biologists may be useful.

Software and code

Policy information about availability of computer code

Data collection	ImageLab (Bio-Rad). This is listed in the Methods section.
Data analysis	FlowJo, BioAnalyzer, CRISPR Genome Analyzer, GraphPad's Prism7, and Image J (NIH). They are listed in the Methods section.

For manuscripts utilizing custom algorithms or software that are central to the research but not yet described in published literature, software must be made available to editors/reviewers upon request. We strongly encourage code deposition in a community repository (e.g. GitHub). See the Nature Research guidelines for submitting code & software for further information.

Data

Policy information about availability of data

All manuscripts must include a data availability statement. This statement should provide the following information, where applicable:

- Accession codes, unique identifiers, or web links for publicly available datasets
- A list of figures that have associated raw data
- A description of any restrictions on data availability

The authors declare that all data supporting the findings of this study are available within the paper and its Supplementary Information.

Field-specific reporting

Please select the best fit for your research. If you are not sure, read the appropriate sections before making your selection.

☒ Life sciences ☐ Behavioural & social sciences ☐ Ecological, evolutionary & environmental sciences

For a reference copy of the document with all sections, see nature.com/authors/policies/ReportingSummary-flat.pdf

Life sciences study design

All studies must disclose on these points even when the disclosure is negative.

Sample size	No statistical methods were used to predetermine sample sizes, but our sample sizes are similar to those generally employed in the field.
Data exclusions	None of the data were excluded for the analysis.
Replication	Each experiment was replicated multiple times and the results were successfully reproduced.
Randomization	Control and injected mice were chosen randomly. We randomized the injection side (left or right side of the brain) for Thy1-YFP or Ai9 mice.
Blinding	The investigator was not blinded to the group of allocation during the experiment and when assessing the outcome. However, behavioral experiments were performed and analyzed as blind.

Reporting for specific materials, systems and methods

Materials & experimental systems

n/a	Involved in the study
☒	☐ Unique biological materials
☐	☒ Antibodies
☐	☒ Eukaryotic cell lines
☒	☐ Palaeontology
☐	☒ Animals and other organisms
☒	☐ Human research participants

Methods

n/a	Involved in the study
☒	☐ ChIP-seq
☐	☒ Flow cytometry
☒	☐ MRI-based neuroimaging

Antibodies

Antibodies used	The mouse monoclonal RFP antibody (6G6) was purchased from ChromoTek; the chicken polyclonal GFP antibody (GFP-1020) from Aves Labs (Tigard, OR); the rabbit polyclonal GFAP antibody (AB5804) and the mouse monoclonal NeuN antibody (MAB377) from Millipore (Burlington, MA) the rabbit polyclonal Iba1 antibody (019-19741) from Wako Chemicals (Richmond, VA); and the rabbit polyclonal mGluR5 antibody (AGC-007) from Alomone Labs (Israel). The goat anti-mouse IgG2a-Cy3, goat anti-chicken-Cy2, goat anti-rabbit-Cy5, goat anti-mouse IgG1-Cy5, and donkey anti-rabbit IgG-Alexa Fluor 647 antibodies were purchased from Jackson ImmunoResearch Laboratories, Inc (West Grove, PA).
Validation	All antibodies were commercially available and were validated by manufacturers. All antibodies were also validated in immunostaining for mouse brain section in this study.

Eukaryotic cell lines

Policy information about cell lines

Cell line source(s)	HEK293T cells from the Cell Culture Facility at UC Berkeley.
Authentication	HEK293T cell line was authenticated using short tandem repeat (STR) profiling.
Mycoplasma contamination	Mycoplasma test was conducted and the result was negative.
Commonly misidentified lines (See ICLAC register)	No commonly misidentified cell lines were used.

Animals and other organisms

Policy information about studies involving animals; ARRIVE guidelines recommended for reporting animal research

Laboratory animals	Ai9 (in C57BL/6J background), Thy1-YFP (in C57BL/6J background), mdx, wild-type (in FVB background: FVB.129P2-Pde6b+ Tyrc-ch/AntJ), and Fmr1 KO (in FVB background: FVB.129P2-Pde6b+ Tyrc-ch Fmr1tm1Cgr/J) mice were obtained from Jackson Laboratory. The use and care of animals in this study follow the guidelines of the UTHSCSA and UC Berkeley Institutional Animal Care and Use Committee.
Wild animals	This study did not involve wild animals.
Field-collected samples	This study did not involve sample collected in field.

Flow Cytometry

Plots

Confirm that:

☒ The axis labels state the marker and fluorochrome used (e.g. CD4-FITC).

☒ The axis scales are clearly visible. Include numbers along axes only for bottom left plot of group (a 'group' is an analysis of identical markers).

☐ All plots are contour plots with outliers or pseudocolor plots.

☒ A numerical value for number of cells or percentage (with statistics) is provided.

Methodology

Sample preparation	Prepared as described in Methods.
Instrument	Attune NxT Flow Cytometer
Software	FlowJo
Cell population abundance	Cells were abundant
Gating strategy	FSC/SSC gating, live cell gating

☐ Tick this box to confirm that a figure exemplifying the gating strategy is provided in the Supplementary Information.